World Electric Vehicle Journal

MDPI

Article

Single-Wheel Failure Stability Control for Vehicle Equipped with Brake-by-Wire System

Jian Zhou, Yage Di and Xuelong Miao *

School of Mechanical and Automotive Engineering, Shanghai University of Engineering Science, Shanghai 201620, China
* Correspondence: m310121506@sues.edu.cn

Abstract: In order to solve the problem of vehicle stability control after a single-wheel brake failure in the brake-by-wire system, a control strategy of braking force redistribution with a yaw moment is proposed to ensure the braking efficiency and stability of vehicles. In this strategy, a two-layer architecture is adopted. In the upper layer control, a fault factor is introduced to represent the real-time failure degree of the wheel, and the driver's braking intention is perceived through the pedal travel and pedal speed of the driver. The braking force redistribution algorithm of the remaining three wheels is designed based on the wheel failure degree and braking intensity. In the lower control, according to the state parameters of the vehicle, the additional yaw moment, which controls the yaw rate and the sideslip angle of the vehicle, is calculated by using the sliding mode control theory, and the yaw moment is reasonably allocated to the normal wheel. By using MATLAB/Simulink and Carsim co-simulation, different braking strength and failure types are selected for simulation analysis. The simulation results show that the proposed control strategy can improve the braking efficiency and stability of the vehicle under different braking conditions.

Keywords: braking-by-wire system; single-wheel brake failure; sliding mode control; braking force redistribution; stability control

Citation: Zhou, J.; Di, Y.; Miao, X. Single-Wheel Failure Stability Control for Vehicle Equipped with Brake-by-Wire System. *World Electr. Veh. J.* **2023**, *14*, 177. https://doi.org/10.3390/wevj14070177

Academic Editor: Kaushik Rajashekara

Received: 31 May 2023
Revised: 24 June 2023
Accepted: 3 July 2023
Published: 4 July 2023

1. Introduction

Safety, energy efficiency, and intelligence are the new trends in the development of future vehicles, and the market of electric vehicles has been gradually increasing in the past few years [1]. Many researchers are focused on the safety of electric vehicles [2], and a key measure to improve vehicle safety is to improve the braking system and braking performance of the vehicle [3]. Among them, the brake-by-wire system not only solves a series of problems brought about by traditional brake systems, such as large volume and slow response, but also brings new opportunities for the rapid development of automotive braking. The Electro-Mechanical Brake (EMB) [4,5] system abandoned the traditional hydraulic braking system by controlling the brake line pressure to control the braking torque and instead used the motor to brake, which acts directly on the caliper end to push the piston to generate the braking torque. Since the EMB uses a wheel side motor for individual braking, the braking force of four wheels can be controlled separately, and the motor control accuracy is higher and faster than traditional hydraulic control, so the braking force can be controlled more accurately [6]. At the same time, however, due to the increased complexity of actuators and systems, the EMB system eliminates the hydraulic backup of traditional vehicles, and the risk of failure of the brake-by-wire system increases. Therefore, it is particularly important to study the single-wheel failure stability control for vehicles equipped with brake-by-wire systems.

For the problem of vehicle stability control when single-wheel braking fails, scholars' research is roughly divided into two categories: the first category is to achieve vehicle stability control by reconfiguring the remaining three-wheel braking force under low braking intensity; the second category is to combine braking and steering systems to achieve vehicle stability control under high braking intensity. For the braking force redistribution problem after single-wheel braking failure, the same side wheel is first used to compensate for the lost braking force when the same side wheel is not enough to compensate for the lost braking force. Then, the different side wheels compensate [7,8], and according to the same side of the wheel that can compensate, three wheels can compensate, three wheels cannot compensate, and the braking intensity is divided into light braking, moderate braking, and severe braking [9]. In [7], the authors took left front wheel failure as an example, and the braking force lost by the left front wheel of a vehicle was compensated by the left rear wheel. When the braking intensity increased to the point that the left rear wheel was no longer enough to compensate for the braking force lost by the left front wheel, the lost braking force continued to be compensated by the right wheel, and the growth rate of the braking force of the right wheel was set inversely proportional to the square of the vehicle speed. This method allows the driver enough time to control the car to implement reverse steering. By setting thresholds, the literature [10] has gradually established the balance of braking force on both sides of the wheel, providing sufficient time for the driver to respond and implement steering, which not only enables the driver to maintain control of the car but also does not significantly increase the braking distance.

For stability control after single-wheel brake failure, a fault-tolerant control structure for a brake-by-wire vehicle equipped with hub motors is designed in [11]. Combined with the regenerative braking system, a sliding mode control algorithm is used to calculate the compensated yaw moment, and a good control effect is achieved. In [12], a practical nonlinear model predictive controller is designed to achieve the trajectory tracking of an unmanned vehicle, the experimental results show that this method has better precision and computational efficiency than the standard MPC controller, and the controller performance is superior. The authors in [13] improved the existing path-following controllers based on adaptive control and synthesized a model reference adaptive controller based on a non-quadratic Lyapunov function. The robust gain-scheduling control problem for autonomous path-tracking systems with random network-induced delay is studied in [14], and an autonomous ground vehicle robust gain-scheduling path-tracking control method considering uncertain tire dynamics, random network delay, and varying vehicle velocity is proposed. In [15], the author used a sliding mode control algorithm to track the yaw rate to obtain an additional yaw moment and used an optimization design method to allocate an additional yaw moment to the other three wheels with normal braking. However, only the failure control under light braking was considered, and the research results of medium and heavy braking failure scenarios are lacking. The research in [16] proposed to take the yaw rate as the control target and used a PID controller to track the yaw rate to obtain the compensated yaw moment and distribute the compensated yaw moment among the remaining three wheels to prevent the vehicle from running off. The authors in [17] adopted coordinated control of the active steering and braking system based on a control distribution algorithm to realize vehicle stability control under single-wheel braking failure conditions. In [18], when a single wheel has a tire blow-out, because the performance of the tire changes after the tire blow-out, the braking force differs greatly from that of the reference model. Therefore, a sliding mode controller is designed to control the angle of the front wheel with yaw rate as the reference, and the differential braking method is adopted to redistribute the braking force, thus achieving the braking stability of the vehicle after a tire failure on a low-braking-strength and high-adhesion-coefficient road surface. The study in [19] conducted simulation experiments on the actuator failure control of the traditional hydraulic braking system and controlled the yaw rate by controlling the steering system. This method is also applicable to distributed-drive electric vehicles with brake-by-wire systems. The authors in [20] studied the stability of the hub motor of distributed-drive electric vehicles after braking failure and used fuzzy PI and fuzzy PD controllers of parallel operation to adjust the braking force of vehicles to ensure the normal running track of distributed vehicles after the failure of the hub motor.

Most of the above studies only considered the case of complete failure of a single wheel of the BBW system vehicle, and when the vehicle brake fails but not completely, if the braking force of the faulty wheel is directly set to zero, it will cause the difference in braking torque between the left and right sides of the vehicle to be too large and result in a large lateral offset of the vehicle [21]. In view of this, this paper introduces a failure factor to characterize the four-wheel failure state and to represent an input parameter for the failure control strategy. The vehicle's center of gravity shifts forward during braking, resulting in an increased load on the front axle wheels, so the front axle wheels produce more damage when they fail [22]. Therefore, the research in this paper takes the left front wheel failure as an example and designs a control strategy for braking force redistribution with an additional yaw moment to ensure the braking effectiveness and body stability of the vehicle in the event of single-wheel failure.

In order to overcome the limitations of the previous scholars' research and fully consider the need for functional safety of the braking system, this control strategy is designed with a dual-layer architecture, and the control logic is shown in Figure 1. According to the failure degree of the brake motor and the desired braking intensity of the driver, the upper controller redistributes the base braking force to meet the total braking force demand and the left and right braking force balance demand. The lower controller used sliding mode control theory to calculate the required additional yaw moment based on the deviation in the ideal and actual values of the vehicle yaw rate and sideslip angle and transmits this moment to the differential brake controller. The differential brake controller distributes the additional yaw moment reasonably to the three wheels in normal operation, thus achieving the purpose of optimal control of the transverse and longitudinal when the single-wheel brake fails.

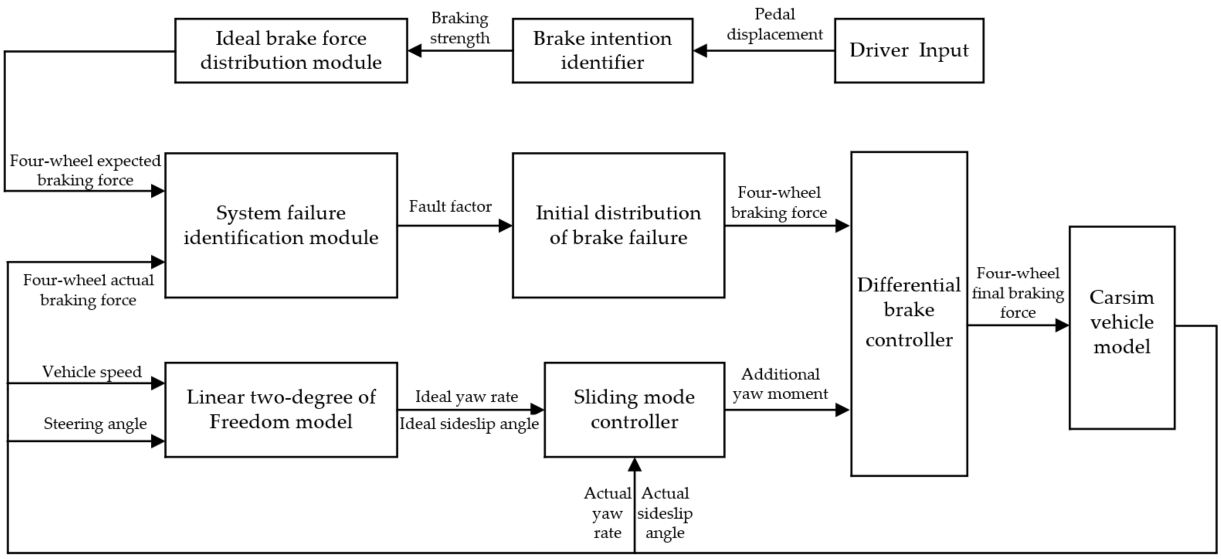

Figure 1. The block diagram of the control strategy.

2. Vehicle Model and Tire Model

2.1. 7-DOF Vehicle Model

Generally, the longitudinal motion, lateral motion, and yaw motion are considered in the coordinated stability control of vehicle braking. However, the front and rear wheel loads shift during braking or acceleration, so the vertical load of the wheel is a time-varying parameter during braking. In order to completely analyze the force on the vehicle after single-wheel failure, a 7-DOF vehicle model is established for simulation analysis by referring to the reference [23]. Figure 2 shows the vehicle dynamics model based on the 3-DOF model of the vehicle's longitudinal, lateral, and yaw, which considers the rotation of four wheels, and ignores the roll motion, pitch motion, and the effect of suspension on the vehicle.

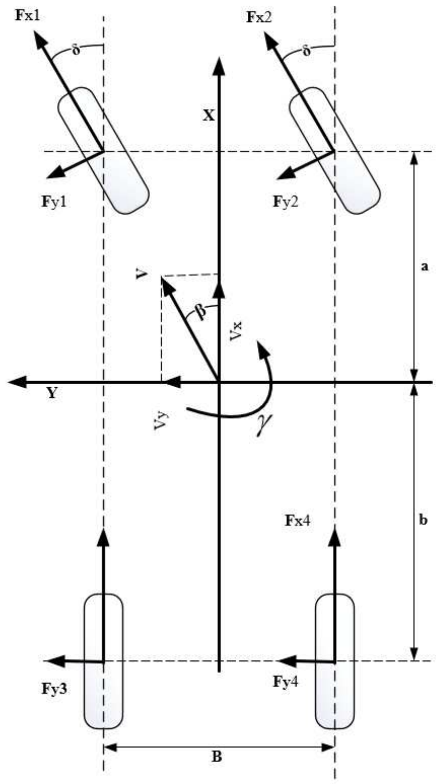

Figure 2. The seven degrees-of-freedom (DOFs) vehicle mode.

The dynamic equations of longitudinal motion, lateral motion, and yaw motion of the vehicle model along the X, Y, and Z directions are as follows.

Longitudinal motion:

$$m(\dot{V}_x - \gamma \cdot V_y) = (F_{x1} + F_{x2})\cos\delta - (F_{y1} + F_{y2})\sin\delta + F_{x3} + F_{x4} \tag{1}$$

Lateral motion:

$$m(\dot{V}_y + \gamma \cdot V_x) = (F_{x1} + F_{x2})\sin\delta + (F_{y1} + F_{y2})\cos\delta + F_{y3} + F_{y4} \tag{2}$$

Longitudinal motion:

$$\begin{gathered} I_z\dot{r} = a(F_{x1} + F_{x2})\sin\delta + a(F_{y1} + F_{y2})\cos\delta + \frac{B}{2}(F_{y1} - F_{y2})\sin\delta - (F_{y3} + F_{y4})b + \\ \frac{B}{2}(F_{x2} - F_{x1})\cos\delta + \frac{B}{2}(F_{x4} - F_{x3}) \end{gathered} \tag{3}$$

In Equations (1)–(3), δ is the front wheel angle, V_x is the longitudinal velocity of the vehicle, V_y is the lateral velocity of the vehicle, γ is the yaw rate, F_{xi} is the longitudinal force of each wheel, and F_{yi} is the lateral force of each wheel. Subscripts 1, 2, 3, and 4 represent the left front wheel, right front wheel, left rear wheel, and right rear wheel, respectively. m is the mass of the vehicle. a is the distance from the center of gravity to the front axle. b is the distance from the center of gravity to the rear axle. B is the wheelbase. I_z is the moment of inertia of the vehicle.

2.2. Tire Model

The "magic formula" tire model of Carsim is selected, which has a good description of the mechanical characteristics of tires under different working conditions [24]. Its basic form is as follows:

$$\mathrm{y} = D\sin\{\mathrm{C}\arctan[Bx - E(Bx - \arctan Bx]\} \tag{4}$$

where D is the peak factor; C is the shape factor; B is the stiffness factor; E is the curvature factor; x is the independent variable, such as the tire side slip angle or the longitudinal slip rate, where D, C, and E are influenced by the vertical load of the tire.

During the movement of the vehicle, the vertical load on the tire changes when affected by longitudinal acceleration and lateral acceleration. The formula is as follows:

$$\begin{aligned}
F_{z1} &= \tfrac{m \cdot a}{2L} g - \tfrac{m \cdot h}{2L} \dot{V}_x - \tfrac{m \cdot h \cdot b}{c \cdot L} \dot{V}_y \\
F_{z2} &= \tfrac{m \cdot b}{2L} g - \tfrac{m \cdot h}{2L} \dot{V}_x + \tfrac{m \cdot h \cdot b}{c \cdot L} \dot{V}_y \\
F_{z3} &= \tfrac{m \cdot a}{2L} g + \tfrac{m \cdot h}{2L} \dot{V}_x - \tfrac{m \cdot h \cdot a}{c \cdot L} \dot{V}_y \\
F_{z4} &= \tfrac{m \cdot a}{2L} g + \tfrac{m \cdot h}{2L} \dot{V}_x + \tfrac{m \cdot h \cdot a}{c \cdot L} \dot{V}_y
\end{aligned} \tag{5}$$

where m is the vehicle mass; h is the height of vehicle centroid; F_{zi} is the vertical load of the tire labeled i; $i = 1, 2, 3, 4$ represent left front, right front, left rear, and right rear wheels, respectively; and L is the distance between the front and rear axles.

3. Braking Force Redistribution Strategy

3.1. Braking Intention Recognition

In order to achieve the desired braking effect of the driver, it is necessary to recognize the driver's braking intention. When the vehicle is braking, the pedal sensor senses the position and changing speed of the pedal through the driver stepping on the brake pedal and transmits the sensor information to the braking central control module. The central control module calculates the optimal braking force required by each wheel in real-time according to this information. This paper adopts the brake intention recognition method based on fuzzy rules [25]. Since pedal displacement X and its change rate can reflect the driver's brake intensity the first time, it is used as the identification parameters of the brake intention identifier to obtain the driver's braking intention and desired braking intensity in real-time and completes the recognition of the driver's braking intention. The braking intention recognition model built on the Simulink platform based on fuzzy rules is shown in Figure 3.

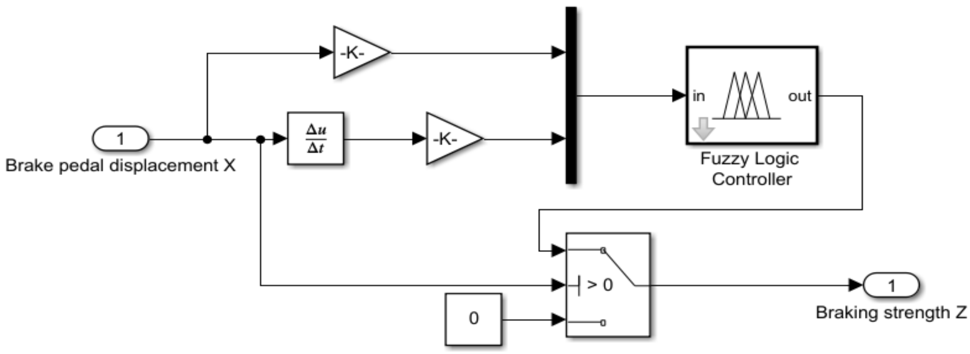

Figure 3. Brake intention recognition model.

3.2. Ideal Braking Force Distribution

When the car is braking, according to the front and rear axle brake braking force distribution, load, road adhesion coefficient, slope, and other factors, and when the front and rear wheels of the car meet the braking requirements, there will be three special braking conditions: the front wheel is locked before the rear wheel, the rear wheel is locked before the front wheel, and the front and rear wheels are locked at the same time. Regardless of whether the front wheel is locked first or the rear wheel is locked first, the attachment condition cannot be maximized. The ideal braking force distribution curve can reasonably distribute the braking force between the front and rear wheels of the vehicle so that the front and rear wheels of the vehicle are locked at the same time [26]. In this case, the braking performance and handling stability of the vehicle have been greatly improved. The specific distribution rules are as follows:

$$\begin{cases} F_{rear} = \frac{1}{2}\left(\frac{G}{h_g}\sqrt{b^2 + \frac{4hL}{G}F_{front}} - \frac{Gb}{h} - 2F_{front}\right) \\ F_{front} + F_{rear} = \varphi G \end{cases} \tag{6}$$

where F_{front} and F_{rear} are front axle wheel braking force and rear axle wheel braking force, respectively; G is the vehicle gravity; and φ is the road adhesion coefficient.

When the braking intensity is Z obtained by the brake intention identifier, the total braking force of the vehicle and the ideal braking force of each wheel are

$$\begin{cases} F_{total} = M \cdot Z; \\ F_{x1} = \frac{1}{2}F_{front}; \\ F_{x2} = \frac{1}{2}F_{front}; \\ F_{x3} = \frac{1}{2}F_{rear}; \\ F_{x4} = \frac{1}{2}F_{rear}; \end{cases} \tag{7}$$

where F_{total} is the total braking force of the vehicle; M is the vehicle mass; F_{x1}, F_{x2}, F_{x3}, and F_{x4}, respectively, are the left front, right front, left rear, and right rear wheel braking force, respectively

3.3. Initial Distribution of Brake Failure

When the vehicle is braking, the system failure recognition module determines whether a wheel failure has occurred by comparing the braking force of each wheel with the expected braking force and introduces the failure factor to characterize the degree of wheel failure when a failure occurs. When braking force loss occurs to the left front wheel, the actual braking force of the wheel is $F'_{x1} = \lambda_{x1} \cdot F_{x1}$, where λ_{x1} represents the failure factor of the failed wheel. For example, when $\lambda_{x1} = 1$, it means normal braking of the wheel; when $\lambda_{x1} = 0.7$, it means that 30% of the braking force of the wheel is lost. In order to satisfy both the braking deceleration and the vehicle stability after single-wheel failure of the brake-by-wire system, the braking force is redistributed to the remaining three wheels based on the failure factor of the failed wheel.

(1) When the desired braking deceleration rate is low, or the braking failure degree of the wheel is small, the braking force lost by the left front wheel due to brake failure can be compensated by the left rear wheel, at which time the braking force of each wheel is

$$\begin{cases} F'_{x1} = F_{x1} - (1 - \lambda_{x1})F_{x1} \\ F'_{x2} = F_{x2} \\ F'_{x3} = F_{x3} + (1 - \lambda_{x1})F_{x1} \\ F'_{x4} = F_{x4} \end{cases} \tag{8}$$

(2) When the desired braking force is larger, or the braking force failure of the wheels is higher, the braking force lost by the left front wheel due to brake failure cannot be completely compensated by the left rear wheel, and the part that cannot be compensated should be compensated by the right wheels. At the same time, in order to minimize the yaw moment caused by the imbalance of the left and right braking force, the braking force provided by the left rear wheel should reach its limit. The remaining braking force that cannot be compensated should be distributed to the right front wheel and the right rear wheel according to the braking force distribution ratio of the front and rear axles. At this time, the braking force of each wheel is

$$\begin{cases} F'_{x1} = F_{x1} - (1-\lambda_{x1})F_{x1} \\ F'_{x2} = F_{x2} + \frac{F_{x2}[(1-\lambda_{x1})F_{x1} - (F_{3m} - F_{x3})]}{F_{x2}+F_{x4}} \\ F'_{x3} = F_{3m} \\ F'_{x4} = F_{x4} + \frac{F_{x4}[(1-\lambda_{x1})F_{x1} - (F_{3m} - F_{x3})]}{F_{x2}+F_{x4}} \end{cases} \tag{9}$$

(3) When the desired braking strength is large, at this time, the three normal wheels have reached the limit of their respective braking force, the braking force lost by the left front wheel due to braking failure cannot be compensated by the three normal wheels, the vehicle cannot reach the driver's desired braking deceleration, and runaway is more significant. The braking force of each wheel is

$$\begin{cases} F'_{x1} = F_{1m} - (1-\lambda_{x1})F_{1m} \\ F'_{x2} = F_{2m} \\ F'_{x3} = F_{3m} \\ F'_{x4} = F_{4m} \end{cases} \tag{10}$$

The peak road adhesion coefficient limits the maximum deceleration that can be achieved by the vehicle while satisfying the braking strength so that the maximum braking force of the wheels needs to meet the constraint [27]:

$$F_{im} = \mu \cdot F_{zi} \tag{11}$$

where F_{im} is the maximum braking force of the wheel and μ is the road peak adhesion coefficient.

4. Yaw Moment Controller

4.1. Reference Model

Referring to the literature [21], a two-degree-of-freedom vehicle dynamics model is established as a vehicle stability reference model, as shown in Figure 4. The ideal yaw rate is obtained by solving at the steady state of the vehicle.

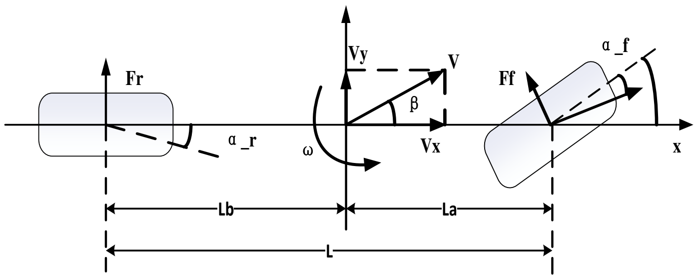

Figure 4. The two-degrees-of-freedom (DOFs) vehicle mode.

According to the model in Figure 4, the motion equation of the two-degrees-of-freedom model can be obtained:

$$\begin{cases} mu\left(\dot{\beta} + \omega\right) = (K_1 + K_2)\beta + \frac{1}{u}(aK_1 - bK_2)\omega - K_1\delta \\ I_Z\dot{\omega} = (aK_1 - bK_2)\beta + \frac{(a^2K_1 + b^2K_2)}{u}\omega - aK_1\delta \end{cases} \tag{12}$$

where β is the sideslip angle; ω is the yaw rate; and K_1 and K_2 are the lateral stiffness of the front and rear wheels, respectively. This equation is rewritten into an equation of state in the form:

$$\begin{bmatrix} \dot{\beta} \\ \dot{\omega} \end{bmatrix} = \begin{bmatrix} \frac{K_1+K_2}{mu} & -1 + \frac{aK_1 - bK_2}{mu^2} \\ \frac{aK_1 - bK_2}{I_Z} & \frac{a^2K_1 + b^2K_2}{I_Z u} \end{bmatrix} \begin{bmatrix} \beta \\ \omega \end{bmatrix} + \begin{bmatrix} -\frac{K_1}{mu} \\ -\frac{aK_1}{I_z} \end{bmatrix} \delta \tag{13}$$

From Equation (13), it can be seen that the two-degree-of-freedom model of the vehicle is mainly composed of the motion of the sideslip angle and yaw rate. When the vehicle is in a steady state, the relationship between the desired yaw rate of the vehicle and the front-wheel angle can be deduced as follows:

$$\omega_d = \frac{u}{L(1+Ku^2)}\delta \tag{14}$$

where K is the stability factor:

$$K = \frac{m}{(a+b)^2}\left(\frac{a}{K_2} - \frac{b}{K_1}\right) \tag{15}$$

According to Equation (14), it can be seen that when the front wheel angle increases, the expected yaw rate will also increase continuously. However, due to the limited value of adhesion provided by the road surface, when the yaw rate increases to exceed the limit of adhesion provided by the road surface, if the yaw rate continues to increase, the wheel will become destabilized. Therefore, the ideal yaw rate is revised as

$$\omega_d = \min\left\{\left|\frac{u}{L(1+Ku^2)}\delta_f\right|, \left|\frac{\mu g}{u}\right|\right\} \cdot \mathrm{sgn}(\delta_f) \tag{16}$$

where μ is the peak road surface coefficient.

The ideal expectation value of the sideslip angle should be zero [28]:

$$\beta_{\mathrm{d}} = 0 \tag{17}$$

When the actual sideslip angle exceeds the set value, or the difference between the actual yaw rate and the ideal yaw rate is too large, the vehicle will lose stability. At this time, the reverse additional yaw moment is applied to bring the vehicle back to the stable state, and the vehicle motion equation is as follows:

$$\begin{bmatrix} \dot{\beta} \\ \dot{\omega} \end{bmatrix} = \begin{bmatrix} \frac{K_1+K_2}{mu} & -1+\frac{aK_1-bK_2}{mu^2} \\ \frac{aK_1-bK_2}{I_Z} & \frac{a^2K_1+b^2K_2}{I_Z u} \end{bmatrix} \begin{bmatrix} \beta \\ \omega \end{bmatrix} + \begin{bmatrix} -\frac{K_1}{mu} \\ -\frac{aK_1}{I_z} \end{bmatrix}\delta + \begin{bmatrix} 0 \\ \frac{1}{I_Z} \end{bmatrix}\Delta M \tag{18}$$

4.2. Additional Yaw Moment Controller

The sliding mode control theory [29,30] has the characteristics of a simple algorithm, strong robustness, and rapid response and is widely used in tracking control of the desired vehicle state. In this paper, sliding mode control is adopted to design the additional yaw moment controller. By simultaneously tracking the yaw rate and the sideslip angle, the additional yaw moment is obtained. The sliding mode surface is defined as

$$s = (\omega - \omega_d) + \zeta(\beta - \beta_d) \tag{19}$$

By differentiating Equation (18), we can obtain

$$\dot{s} = (\dot{\omega} - \dot{\omega}_d) + \zeta(\dot{\beta} - \dot{\beta}_d) \tag{20}$$

where ζ is the sliding mode control parameter, which can be obtained by combining (3), (12), and (20):

$$\dot{s} = \frac{1}{I_z}\left[(aK_1 - bK_2)\beta + \frac{a^2K_1 + b^2K_2}{u}\omega\right] - \frac{1}{I_z}\left(aK_1\delta_f + M\right) - \dot{\omega}_d + \zeta(\dot{\beta} - \dot{\beta}_d) \tag{21}$$

The choice of slip surface and slip control rate determines the effect of slip control, and the slip control rate chosen in this paper is the exponential convergence law:

$$M_{zs} = -\varepsilon \mathrm{sgn}(s) - ks \tag{22}$$

where ε and k are variable parameters greater than 0.

In summary, the additional yaw moment sliding mode controller in this paper is

$$\Delta M = M_b + M_{zs} \tag{23}$$

4.3. Additional Yaw Moment Distribution Strategy

According to the seven-degree-of-freedom model of the whole vehicle established in Figure 2, the unintended steering of the wheels after brake failure will generate lateral and longitudinal forces, and due to the limitation of the road surface adhesion coefficient, the lateral and longitudinal forces of the wheels satisfy the coupling equation:

$$F_x^2 + F_y^2 \leq (\mu F_z)^2 \tag{24}$$

At the initial braking force distribution, in order to achieve the driver's desired braking deceleration, the longitudinal force of the remaining three normal wheels is already close to or even at the adhesion limit. It is known from Equation (24) that the lateral force generated by the unintended steering of the front wheels affects the longitudinal force, which can be derived from Equation (4) for different slip rates and different side deflection angles.

The slip rate of each wheel tire is calculated as follows:

$$\lambda_i = \frac{V_x - \omega_i \cdot R_i}{V_x} \tag{25}$$

The side slip angle of each wheel tire is calculated as follows:

$$\begin{cases} \alpha_1 = \arctan\left(\frac{V_y + a\cdot\gamma}{V_x - B\cdot\gamma/2} - \delta\right) \\ \alpha_2 = \arctan\left(\frac{V_y + a\cdot\gamma}{V_x + B\cdot\gamma/2} - \delta\right) \\ \alpha_3 = \arctan\left(\frac{V_y - b\cdot\gamma}{V_x - B\cdot\gamma/2}\right) \\ \alpha_4 = \arctan\left(\frac{V_y - b\cdot\gamma}{V_x + B\cdot\gamma/2}\right) \end{cases} \tag{26}$$

According to the calculated lateral force F_{yi}, the limit value of the longitudinal force of the wheel is revised as follows:

$$F'_{im} = \sqrt{(\mu \cdot F_{zi})^2 - F_{yi}^2} \tag{27}$$

The additional yaw moment calculated by sliding mode control is distributed to the remaining three normal wheels and uses a three-wheel differential brake to complete the additional yaw moment control. The additional longitudinal force required to achieve the desired additional yaw moment is

$$F_{\Delta x} = \frac{2\Delta M}{B} \tag{28}$$

where $F_{\Delta x}$ is the total longitudinal force required.

In order to maximize the driver's desired braking deceleration, it should be realized by the left rear wheel braking first. When the left rear wheel reaches the adhesion limit, the part of the yaw moment that cannot be reached is realized by the different side wheels, and the vertical load ratio of the front and rear wheels is used to distribute the front and rear wheel braking torque relationship. The specific distribution rules are as follows:

$$\begin{cases} F_{\Delta x3} = F'_{3m} - F'_{x3} \\ F_{\Delta x2} = -\frac{F_{z2}}{\cos\delta(F_{z2}+F_{z4})}\left(\frac{2\Delta m}{B} - F_{\Delta 3}\right) \\ F_{\Delta x4} = -\frac{F_{z4}}{(F_{z2}+F_{z4})}\left(\frac{2\Delta m}{B} - F_{\Delta 3}\right) \end{cases} \tag{29}$$

The target braking force of each wheel should be no greater than the maximum braking force:

$$F_{xi\_obj} = F'_{xi} + F_{\Delta xi}, F_{xi\_obj} \le F'_{im} \tag{30}$$

5. Simulation and Analysis

In this paper, Simulink and Carsim co-simulation is used to verify the braking force distribution and additional yaw moment control strategy after single-wheel failure. The B-class car in Carsim is taken as the reference car, the corresponding parameters are modified on this basis, and the braking system is changed to four-wheel independent braking. The main parameters of the vehicle are set as shown in Table 1.

Table 1. Main parameters used in the simulations.

Vehicle Parameters	Value
Vehicle weight (m/kg)	1651
Distance from front axle to center of mass (a/m)	1.595
Distance from rear axle to center of mass (b/m)	1.365
Moment of inertia of the vehicle (I_Z / (kg·m^2))	1536.7
Wheel pitch (B/m)	1.675
Wheel radius (R/m)	0.31
Centroid height (h_g /m)	0.5718
Front wheel lateral stiffness (K_1 / (N·rad^{-1}))	107,610
Rear wheel lateral stiffness (K_2 / (N·rad^{-1}))	74,520
Effective radius of brake disc (r_b /m)	0.16
Road adhesion coefficient (μ)	0.8

In this study, the straight and curve road was selected, the road adhesion coefficient was set as 0.8, and the simulation time was set as 2 s after the single-wheel brake failure occurred. The simulation conditions were complete failure ($\lambda_{x1} = 0$) of left front wheel braking in light braking ($Z = 0.3$ g), partial failure ($\lambda_{x1} = 0.7$), and complete failure ($\lambda_{x1} = 0$) of the left front wheel in emergency braking ($Z = 0.7$ g), and the initial speed of the vehicle was set as 110 km/h. Under the two conditions, with or without the intervention of control strategy, the changes in vehicle braking parameters and stability parameters, such as braking deceleration, lateral offset, yaw rate, and sideslip angle, were compared and analyzed to verify the effectiveness and response speed of the control strategy and provide directional guidance for the optimization of the control strategy. The results and analysis are as follows.

5.1. Light Braking When Driving in a Straight Line with Complete Failure of the Left Front Wheel Brake

As can be seen from Figure 5, under the light braking situation, when the braking force of the left front wheel of the vehicle completely fails, due to the imbalance of the braking force of the left and right sides wheels, the vehicle suffers serious instability, and the maximum yaw rate and the sideslip angle reach 4 deg/s and 0.6 deg, respectively, in 2 s. In this process, the lateral offset changes sharply and finally reaches 2.5 m, and the vehicle runs off rapidly. Due to the loss of wheel braking force, the braking deceleration of the vehicle is reduced to 0.2 g. At this time, the vehicle is running at a high speed, which will bring great danger to itself and the people in the surrounding vehicles. When the failure control strategy is involved, because the left front wheel loses less braking force due to braking failure, the system compensates for the lost braking force by redistributing the braking force of the remaining three wheels and carries out stability control with the additional yaw moment according to the vehicle state. As can be seen from Figure 5a,d, the run-off distance is controlled from 2.5 m to less than 0.2 m within 2 s. After failure control, the braking deceleration reaches 0.29 g, which meets the driver's expectation of 0.3 g braking deceleration to the greatest extent. According to Figure 5b,c, after the additional yaw moment is applied, the yaw rate is stabilized below ±0.5 deg/s within 1 s, and the sideslip angle is also limited within 0.1 deg. Compared with the vehicle without control, the control strategy can effectively reduce the yaw rate and sideslip angle to avoid complete instability of the vehicle. The vehicle can be kept in a safe condition.

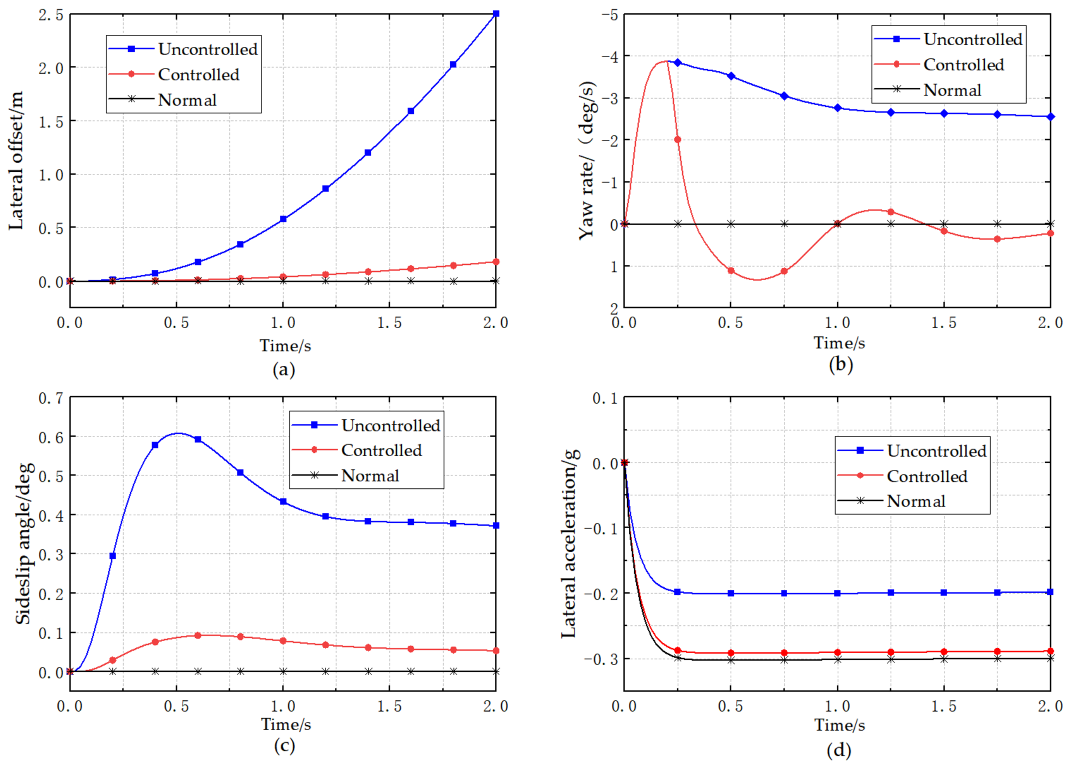

Figure 5. Simulation results of light braking with complete failure of left front wheel: (**a**) lateral offset; (**b**) yaw rate; (**c**) sideslip angle; (**d**) lateral acceleration.

5.2. Emergency Braking When Driving in a Straight Line with the Left Front Wheel Brake Failed 30%

According to the simulation results, in the case of emergency braking, the braking force of the left front wheel partially fails, and the braking force is 70% of that under normal conditions. In this case, the braking force of the vehicle cannot reach the expected braking force. As can be seen from Figure 6d, the braking deceleration of the vehicle at this time is only 0.6 g. The partial loss of braking force of the left front wheel will not only affect the braking deceleration but also cause instability of the vehicle due to the imbalance of braking force on the left and right sides, making the driving direction of the vehicle deviate from the expected route. As can be seen from Figure 6a–c, the lateral offset of the vehicle reaches nearly 1.2 m within 2 s, and the yaw rate and the sideslip angle both increase greatly. The maximum is 3.6 deg/s and 0.5 deg, respectively. The vehicle has a slight destabilization, but because the vehicle is in a state of high speed at this time, the partial failure of the single wheel will also cause greater harm to the driver and passengers. It can be seen from Figure 6d that after the control strategy intervention, through the redistribution of braking force, the braking force of the vehicle can reach the desired braking force, and the braking deceleration of the vehicle basically meets 0.7 g. At the same time, the additional yaw moment applied effectively reduces the yaw rate and sideslip angle at the turning point, and the lateral stability of the vehicle is greatly improved so that it can follow the expected path to brake and decelerate. As can be seen from Figure 6a–c, the yaw rate and the sideslip angle decrease from 2 deg/s to 0.24 deg/s and 0.3 deg to 0.04 deg, respectively, and the lateral offset decreases from 1.2 m to 0.1 m, indicating that the vehicle is basically in the same state as before the failure. The safety of drivers and passengers is greatly ensured.

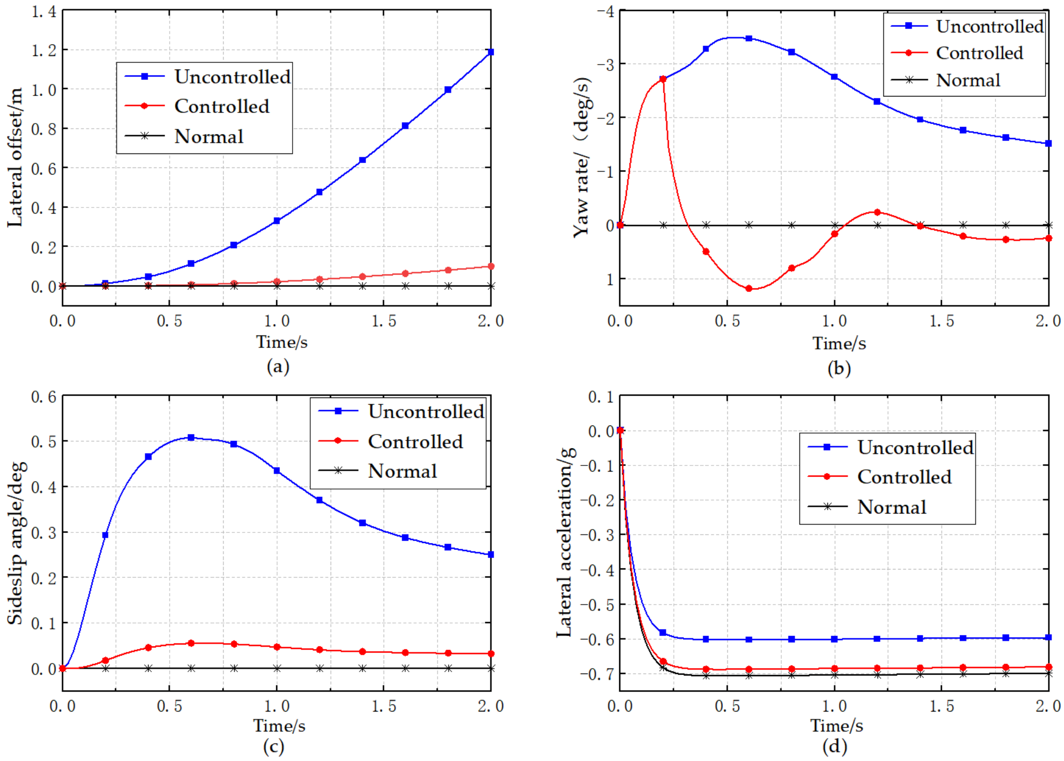

Figure 6. Simulation results of emergency braking with 30% left front wheel failure: (**a**) lateral offset; (**b**) yaw rate; (**c**) sideslip angle; (**d**) lateral acceleration.

5.3. Emergency Braking When Driving in a Straight Line with Complete Failure of the Left Front Wheel Brake

As can be seen from Figure 7, the left front wheel fails completely under emergency braking, and the braking deceleration fluctuates greatly due to the other three normal wheels locking, dropping to 0 within 2 s. During this process, the lateral offset of the vehicle reaches 5.5 m, and the yaw rate and the sideslip angle also increase sharply, reaching a maximum of 80 deg/s and 1.8 deg, indicating that the vehicle is experiencing serious instability and tail-throwing. In real life, uncontrolled vehicles can cause serious traffic accidents. When the control strategy is involved, it can be seen from Figure 7d that through the redistribution of braking force, the braking deceleration recovers and remains stable, but there is still a certain difference between the braking deceleration of the vehicle and the driver's desired braking deceleration, and it is finally maintained at about 0.55 g due to the limitation of the road adhesion coefficient and the sacrifice of a part of braking force to ensure stability. However, the reconstruction of the braking force results in a large yaw moment of the vehicle, as can be seen from the simulation results in Figure 7a–c. At the initial stage of the control strategy intervention, the braking force on the left and right sides is still unbalanced after the redistribution of braking force, and the yaw rate is still at a high value, reaching 10 deg/s. After continuous modification of the additional yaw moment, within 0.5 s after the intervention of control strategy, the yaw rate is stable below ±3 deg/s, the sideslip angle is no more than 0.2 deg, and the lateral offset of the vehicle is controlled below 0.5 m, indicating that the vehicle has reached a controllable state after control, which greatly improves the safety of vehicle braking.

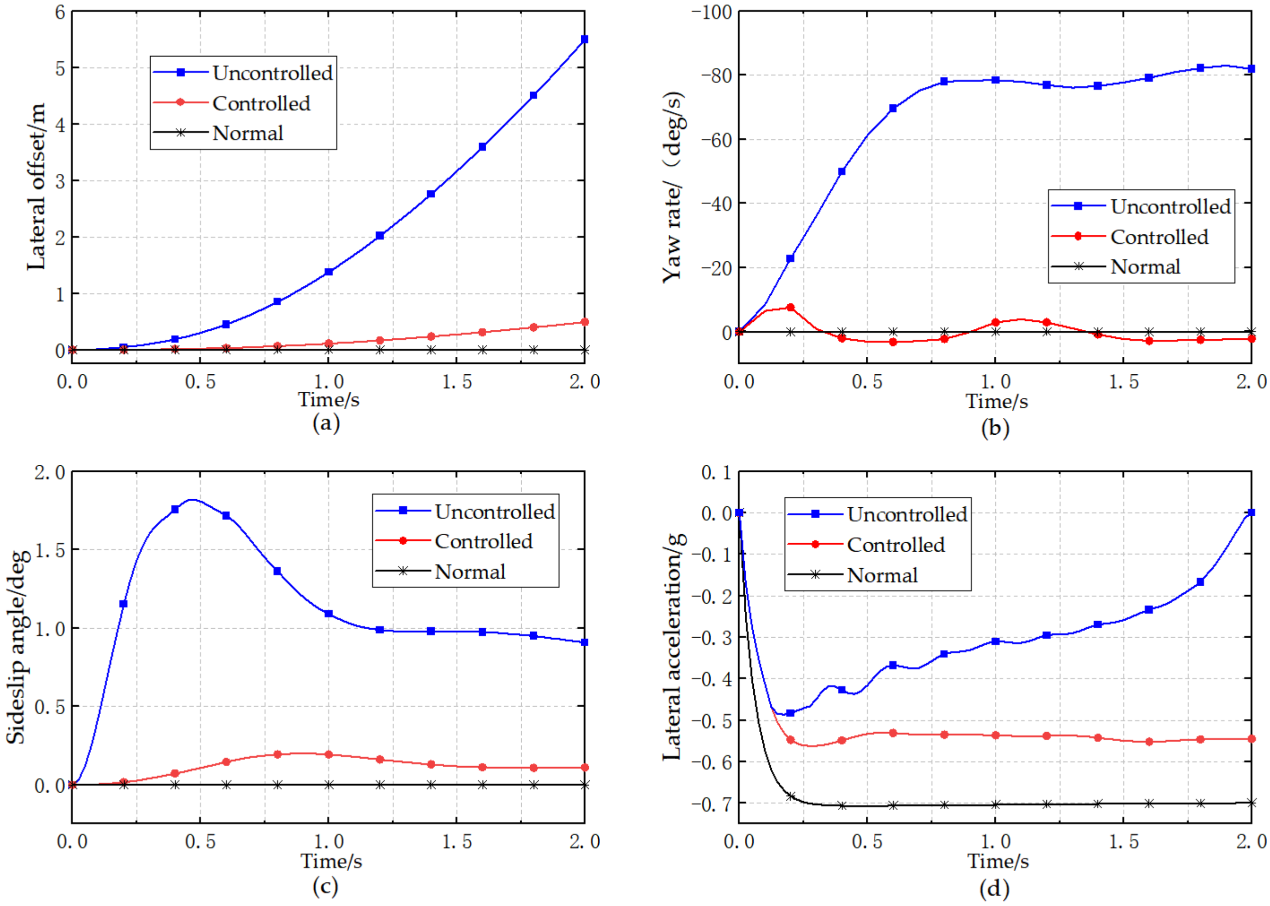

Figure 7. Simulation results of emergency braking with complete failure of left front wheel: (**a**) lateral offset; (**b**) yaw rate; (**c**) sideslip angle; (**d**) lateral acceleration.

5.4. Light Braking When Driving in Turning with Complete Failure of the Left Front Wheel Brake

In order to verify the control effect of the control strategy proposed in this paper under turning conditions, taking the complete failure of the left front wheel during right turning as an example, the vehicle was set to drive at a speed of 110 km/h on the road with a radius of 200 m. As can be seen from the simulation results, the control strategy proposed in this paper can well ensure the safety of the vehicle when the left front wheel brake completely fails during light braking of the vehicle on a curved road. As shown in Figure 8b,c, comparing the state of the failed uncontrolled vehicle and the failed controlled vehicle, it can be seen from the yaw rate and sideslip angle that the failed uncontrolled vehicle generates yaw torque conducive to steering due to the loss of braking force of the left front wheel, thus making the vehicle oversteer, and the yaw rate and sideslip angle are much larger than the value of normal driving. As can be seen from the trajectory of the vehicle in Figure 8a, the failed uncontrolled vehicle deviates from the target track to the inside of the curve, at which point the vehicle is in a state of instability. After the failure control, the vehicle can make up for the lost braking force by reconstructing the braking force of the other three normal wheels while ensuring the braking stability of the vehicle. As can be seen from Figure 8a–c, the vehicle, after failure control, can stably follow the value of normal driving, regardless of the yaw rate and sideslip angle or the vehicle's driving track. As can be seen from Figure 8d, the braking deceleration also returns to a normal value, and the vehicle enters a safe driving state.

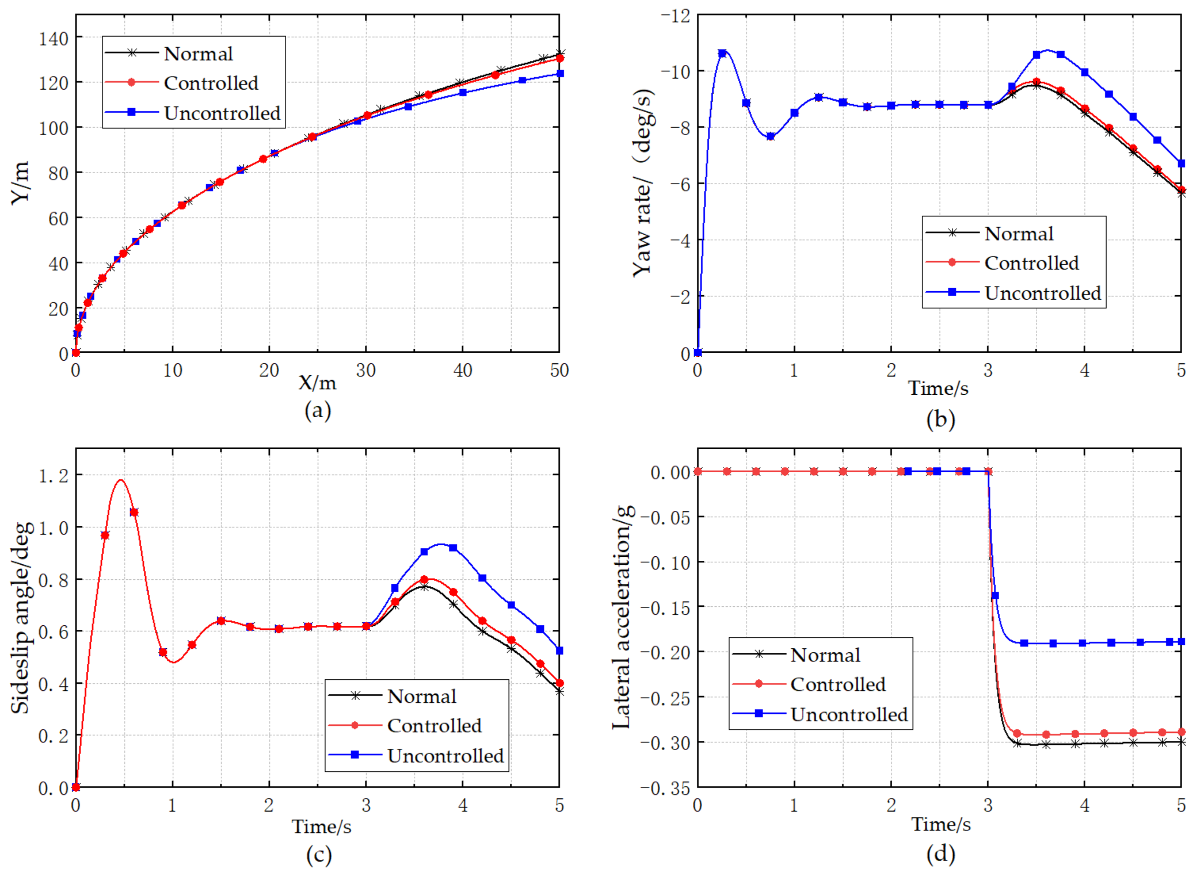

Figure 8. Simulation results of light braking when driving in turning with complete failure of left front wheel: (**a**) path comparison; (**b**) yaw rate; (**c**) sideslip angle; (**d**) lateral acceleration.

6. Conclusions

In this paper, the stability of a single-wheel failure of a brake-by-wire system vehicle is controlled by layers. Firstly, the braking force redistribution algorithm of the remaining three wheels is designed based on the failure factor of the failure wheel, and then the additional yaw moment controller is designed by sliding mode control for yaw rate and sideslip angle. Finally, the effectiveness of the designed control strategy is verified by a co-simulation experiment. The simulation results show that, under light braking and emergency braking conditions, regardless of whether the left front wheel fails completely or partially, the control strategy proposed in this paper can ensure that the vehicle is maintained in a safe and controllable stable state and can satisfy the driver's braking expectation to the maximum extent while ensuring stability, which effectively inhibits the impact of single-wheel braking failure on the vehicle and ensures the safety of the vehicle.

In future studies, the intervention of vehicle active steering during braking failure will be considered, and the effectiveness of the designed failure control strategy will be verified by combining HiL bench and real vehicle tests, which will provide important technical support for the development and application of brake-by-wire systems required for vehicle electrification.

Author Contributions: Conceptualization, J.Z. and Y.D.; methodology, J.Z.; software, X.M.; validation, X.M.; formal analysis, Y.D.; investigation, J.Z.; resources, X.M.; writing—original draft preparation, J.Z.; writing—review and editing, Y.D.; visualization, X.M.; supervision, X.M. All authors have read and agreed to the published version of the manuscript.

Funding: This research received no external funding.

Data Availability Statement: No applicable.

Conflicts of Interest: The authors declare no conflict of interest.

References

1. Mopidevi, S.; Narasipuram, R.P.; Aemalla, S.R.; Rajan, H. E-mobility: Impacts and analysis of future transportation electrification market in economic, renewable energy and infrastructure perspective. *Int. J. Powertrains* **2022**, *11*, 264–284. [CrossRef]
2. Narasipuram, R.P.; Mopidevi, S. A technological overview & design considerations for developing electric vehicle charging stations. *J. Energy Storage* **2021**, *43*, 103225.
3. Xiao, F.; Gong, X.; Lu, Z.; Qian, L.; Zhang, Y.; Wang, L. Design and Control of New Brake-by-Wire Actuator for Vehicle Based on Linear Motor and Lever Mechanism. *IEEE Access* **2021**, *9*, 95832–95842. [CrossRef]
4. Yong, J.; Wang, H.; Dong, J.; Chen, Q.; Zhang, Q. Review on the Research Status and Development Trend of Wire Control Technology. *China Auto* **2022**, *368*, 16–22.
5. Chen, S.; Wang, J.; Zhang, X. Coordinated Control of Braking and Yaw Stability for Vehicle Equipped with Brake-by-Wire System. *J. Univ. Jinan (Sci. Technol.)* **2020**, *34*, 371–376+383.
6. Zuo, B. Research on The KeV Technologies of Controller of Automotive Electromechanical Brake System. Master's Thesis, Zhejiang University, Hangzhou, China, 2014.
7. Huang, Y. Study of Brake Force Distribution Method for Brake-by-Wire System. Master's Thesis, Hunan University, Changsha, China, 2011.
8. Xia, L. The Study on Distributed Hybrid Braking System Based on EMB. Ph.D. Thesis, Chongqing University, Chongqing, China, 2019.
9. Liu, Y. Research on Vehicle Stability Control Strategy of The Brake-by-Wire System Brake Failure. Master's Thesis, Hunan University, Changsha, China, 2017.
10. Hac, A. *Control of Brake- and Steer-by-Wire Systems during Brake Actuator Failure*; SAE Technical Paper; SAE: Warrendale, PA, USA, 2006.
11. Kim, S.; Huh, K. Fault-tolerant braking control with integrated EMBs and regenerative in-wheel motors. *Int. J. Automot. Technol.* **2016**, *17*, 923–936. [CrossRef]
12. Pang, H.; Liu, M.H.; Hu, C.; Liu, N. Practical Nonlinear Model Predictive Controller Design for Trajectory Tracking of Unmanned Vehicles. *Electronics* **2022**, *11*, 1110. [CrossRef]
13. Zhou, X.Y.; Wang, Z.J.; Wang, J.M. Automated Vehicle Path Following: A Non-Quadratic-Lyapunov-Function-Based Model Reference Adaptive Control Approach With e(infinity)-Smooth Projection Modification. *IEEE Trans. Intell. Transp. Syst.* **2022**, *23*, 21653–21664. [CrossRef]
14. Zhao, J.; Li, W.F.; Hu, C.A.; Guo, G.; Xie, Z.C.; Wong, P.K. Robust Gain-Scheduling Path Following Control of Autonomous Vehicles Considering Stochastic Network-Induced Delay. *IEEE Trans. Intell. Transp. Syst.* **2022**, *23*, 23324–23333. [CrossRef]
15. Ji, I.P.; Jeon, K.; Choi, S. Design of fail-safe controller for brake-by-wire systems using optimal braking force distribution. In Proceedings of the Electric Vehicle Symposium & Exhibition, Barcelona, Spain, 17–20 November 2014.
16. Xia, P. Research on Fault Tolerant Control for Brake Execution System of Electromechanical Brake Vehicle. Master's Thesis, Jilin University, Changchun, China, 2012.
17. Wang, M. Fault Diagnosis of the Brake-by-Wire Actuators Sensors and Coordination Control of Vehicle Stability. Master's Thesis, Jilin University, Changchun, China, 2013.
18. Fei, W.; Hong, C.; Cao, D. Nonlinear Coordinated Motion Control of Road Vehicles After a Tire Blowout. *IEEE Trans. Control Syst. Technol.* **2016**, *24*, 956–970.
19. Straky, H.; Kochem, M.; Schmitt, J.; Isermann, R. Influences of braking system faults on vehicle dynamics. *IFAC Proc. Vol.* **2003**, *11*, 337–343. [CrossRef]
20. Sugisaka, M.; Mbaïtiga, Z. Design of PID Fuzzy Controller for Electric Vehicle Brake Control System Based on Parallel Structure of PI Fuzzy and PD Fuzzy. *IEEJ Trans. Ind. Appl.* **2005**, *125*, 245–252. [CrossRef]
21. Li, Q.; Zhang, H.; Shuai, Y.; Chao, G. Single Wheel Failure Stability Control for Four-wheel Independent Drive Electric Vehicles. *Control Eng. China* **2021**, *28*, 155–163.
22. Peng, X.; Wen, K. Control Strategy of Optimal Braking Force Distribution for Vehicle with Brake-by-wire System after Single Wheel Brake Failure. *J. Hunan Univ. (Nat. Sci.)* **2018**, *45*, 44–53.
23. Yang, K.; Dong, D.; Ma, C.; Tian, Z.; Chang, Y.; Wang, G. Stability Control for Electric Vehicles with Four In-Wheel-Motors Based on Sideslip Angle. *World Electr. Veh. J.* **2021**, *12*, 42. [CrossRef]
24. Ou, J.; Yan, D.; Zhang, Y.; Yang, E.; Huang, D. Research on the Stability Control Strategy of Distributed Electric Vehicles Based on Cooperative Reconfiguration Allocation. *World Electr. Veh. J.* **2023**, *14*, 31. [CrossRef]
25. Yang, H.; Ji, F.; Yang, S. Research of Braking Energy Recovery System Based on Simulink-Cruise Combined Simulation. *Control Eng. China* **2018**, *25*, 1086–1090.
26. Zhang, G. Matching and Simulation Analysis of the Braking System. Master's Thesis, Beijing Institute of Technology, Beijing, China, 2016.
27. Cheng, J.; Zheng, K.; Qin, J.; Wu, X. Functional safety analysis and application design of EMB system for intelligent vehicles. *J. Automot. Saf. Energy* **2023**, *14*, 69–79.
28. Li, B.Y.; Du, H.P.; Li, W.H. Fault-tolerant control of electric vehicles with in-wheel motors using actuator-grouping sliding mode controllers. *Mech. Syst. Signal Proc.* **2016**, *72–73*, 462–485. [CrossRef]

29. Song, C.X.; Xiao, F.; Song, S.X.; Li, S.K.; Li, J.H.; Ieee. Stability Control of 4WD Electric Vehicle with In Wheel-Motors Based on Sliding Mode Control. In Proceedings of the IEEE Proceedings Sixth Int Conference Intelligent Control Inform Processing, Wuhan, China, 26–28 November 2015; pp. 251–257.
30. Zhang, D.; Liu, G.H.; Zhou, H.W.; Zhao, W.X. Adaptive Sliding Mode Fault-Tolerant Coordination Control for Four-Wheel Independently Driven Electric Vehicles. *IEEE Trans. Ind. Electron.* **2018**, *65*, 9090–9100. [CrossRef]